IET Image Processing

Research Article

IET Journals
The Institution of Engineering and Technology

Localisation and segmentation of optic disc with the fractional-order Darwinian particle swarm optimisation algorithm

ISSN 1751-9659
Received on 20th October 2017
Revised 12th January 2018
Accepted on 10th March 2018
doi: 10.1049/iet-ipr.2017.1149
www.ietdl.org

Fan Guo[1], Hui Peng[1,2] ✉, Beiji Zou[1], Rongchang Zhao[1], Xiyao Liu[1]

[1]*School of Information Science and Engineering, Central South University, Changsha, Hunan 410083, People's Republic of China*
[2]*Collaborative Innovation Center of Resource-conserving and Environment-friendly Society and Ecological Civilization, Changsha, Hunan 410083, People's Republic of China*
✉ *E-mail: huipeng@mail.csu.edu.cn*

Abstract: Automatic optic disc (OD) localisation and segmentation is still a great challenge in computer-aided diagnosis and screening system. Here, a new OD segmentation algorithm is proposed based on the distinct features of OD in terms of its intensity and shape. The algorithm includes four stages: image preprocessing, image segmentation, ellipse fitting, and OD localisation and segmentation. In the preprocessing stage, the blood vessel in the input retinal image is removed by using the morphological operation and median filtering in HSL (hue–saturation–lightness) colour space. In the image segmentation and ellipse fitting stages, the fractional-order Darwinian particle swarm optimisation algorithm is used to extract the brightest region, and the least-squares optimisation is adopted to detect elliptical OD shape. Finally, the smooth OD borders are generated in the last stage. The proposed method is evaluated by the centroid difference, overlapping ratio, overlap score, and success indexes. Experimental results on the retinal images from DRION, MESSIDOR, ORIGA, and many other public databases demonstrate that the proposed method has superior performance, and may be a suitable tool for automated retinal image analysis.

1 Introduction

The colour fundus images are widely used for checking abnormalities or changes in retina [1]. By observing the shape and variation of optic disc (OD) and retinal blood vessel, some serious eye diseases that may cause blindness, such as glaucoma, cataract, and macular disease, can be detected early, and thus it would become more effective to the clinical treatment. For a colour fundus image, some anatomical structures like the OD, optic cup, blood vessels, and the macula may be contained. The OD in healthy retinal image is the region of the posterior pole where the vasculature and retinal nerve axons enter and leave the eye [2], and the OD generally has two distinct features: (i) the OD appears as a bright yellowish object, and (ii) its shape is like an ellipse. For the first feature, compared with the darker surrounding retinal tissue, the OD appears bright, and the yellowish colour of OD is caused by the absence of the pigmented epithelium in this zone. For the second feature, the elliptical shape provides a useful cue for OD localisation and segmentation. The location of OD is important for many applications [3]. For example, other anatomical structures such as the fovea can be located and segmented by using the OD location as a landmark [4]. Left and right eyes in fovea-centred retinal images can also be classified by using the OD location [5]. Besides, the detection of OD location is very useful for computing some important diagnostic indices for hypertensive retinopathy [6]. Also, the detection of OD location is very important to remove large exudates and lesions from a set of candidate lesions since the OD can be easily confounded with them [7].

Owing to the importance of OD, this paper presents a new OD localisation and segmentation method for retinal images by using the fractional-order Darwinian particle swarm optimisation (FODPSO). The algorithm first removes the blood vessel of retinal image using morphological operation in HSL (hue–saturation–lightness) colour space. Then, the OD candidate region is segmented by using the FODPSO [8, 9] and the region is depicted in elliptical shape by using the least-squares ellipse fitting [2, 10]. Finally, the OD location is refined according to the size of candidate region. Although the individual technique used in both location and segmentation stages are mostly known, the novel aspect of the proposed method is that these techniques are combined for locating the OD in the retinal images, and the experimental results on the data from the public databases demonstrate that the proposed method is quite effective.

The paper is organised as follows. In Section 2, the related works about the localisation and segmentation of OD and the particle swarm optimisation (PSO) are reviewed. Section 3 describes the proposed algorithm in detail. Experimental results of the proposed algorithm on the public image database are discussed in Section 4. In Section 5, we discuss some critical issues related to the proposed algorithm. Finally, we conclude the paper in Section 6.

2 Related work

2.1 OD localisation and segmentation

Recently, many approaches have been proposed to solve the problem of OD localisation and segmentation, the authors in [11, 12] give a detailed review of these approaches. Generally, the OD localisation and segmentation methods can be mainly divided into two categories: model-based methods and appearance-based methods [3]. Model-based methods depend mainly on extracting the blood vessels of the retinal images, and this kind of method regards the location of the OD as the point where all the retinal vessels originate. For example, the success rate of the geometrical model-based method proposed by Foracchia *et al.* [7] is 97.5%, but it takes 2 min to locate the OD for a given image. The vessel's direction matched filter proposed by Youssif *et al.* [12] achieves an accuracy of 98.8%, but it takes ∼3.5 min per image to correctly locate the OD. Lalonde *et al.* [13] proposed a Hausdorff-based template matching technique to locate the OD. Salazar-Gonzalez *et al.* [14] incorporated the blood vessel segmentation into the graph construction to segment OD. Fuzzy convergence of blood vessels to locate the centre of OD was also used in [15]. Although these methods can achieve promising results, they are very time-consuming, since they require retinal vessel segmentation as the initial step of the OD localisation process. Appearance-based methods are based on the observation that the location of the OD is generally the location of the brightest elliptical object within the retinal image. For example, Li and Chutatape [16] used principal component analysis to locate the OD even for retinal images having bright lesions, and the boundary of the OD in this method is

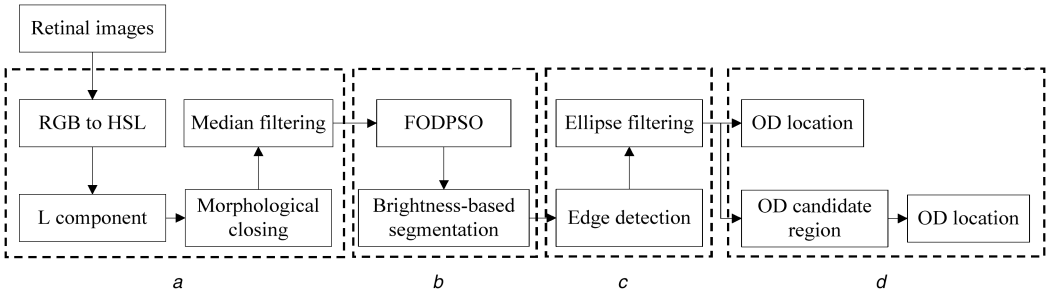

Fig. 1 *Flowchart of the proposed method*
(a) Image preprocessing, ***(b)*** FODPSO-based segmentation, ***(c)*** Ellipse fitting, ***(d)*** OD localisation and segmentation

extracted by a modified active shape model technique. Tjandrasa *et al.* [17] proposed a method to segment OD by using Hough transform and active contour operations. The active contour-based approach combined with mathematical morphology was also used in [18] to automatically segment OD area. Mahfouz and Fahmy [3] obtained two projections of certain image features that encode the x- and y-coordinates of OD, and the resulting one-dimensional (1D) projections are then applied to determine the location of the OD. Sopharak *et al.* [19] used the entropy feature on the intensity component of the contrast-enhanced retinal image to detect OD, since the OD, which is normally smooth, appears in relatively low intensity in entropy space.

For last few years, several researchers have tried introducing PSO and its variants in the area of OD localisation. For example, Devasia *et al.* [1] proposed an automated method to locate and segment the OD in colour fundus images using histogram-based PSO techniques. However, PSO is not the best choice for this purpose, and its variant FODPSO was proved to be more efficient than the PSO algorithm [20]. Koyuncu and Ceylan [21] segmented OD by using a cascade multithresholding procedure. The procedure includes the Scout PSO (ScPSO) algorithm and kapur function. However, the method involves many parameters (e.g. optimum threshold pairs) that need to be tuned according to different input retinal images. Krishna *et al.* [22] tackled the OD segmentation problem by using a shape prior model and a texture prior model, and the PSO algorithm is used to refine the preliminary segmentation according to the shape prior model. However, the method is not automatic, which limits its use in real applications.

2.2 PSO and its improved algorithms

For swarm intelligence, there are two famous algorithms: ant colony optimisation [23] algorithm and PSO [24, 25] algorithm. The latter PSO is inspired by birds flocking or fish school in searching for food. Now the PSO has become an excellent optimisation tool. However, PSO and other optimisation algorithms have a general drawback – they may be trapped in a local optimal solution.

In order to overcome the drawback, Darwinian PSO (DPSO) algorithm was proposed by Tillett *et al.* [26] who introduced the natural selection in PSO. In this algorithm, multiple swarms of test solutions may exist at any time with some rules governing the collection of swarms, which are designed to simulate natural selection [27]. Thus, the ability of searching global optimisation is enhanced by the diversity population of DPSO. FODPSO is an evolutionary algorithm that extends the DPSO using fractional calculus concepts to control the convergence rate [28]. Since the FODPSO can attain memory of past decisions and even better convergence properties compared with PSO and DPSO algorithm, thus the FODPSO algorithm is widely used in many areas, such as hyperspectral image segmentation [29, 30], glioma detection in brain magnetic resonance images [9], and unknown environment exploration of multi-robot system [31]. In this paper, the FODPSO algorithm is used to obtain an appropriate partition for a target retinal image according to the image brightness.

3 Proposed algorithm

3.1 Algorithm overview

The proposed OD localisation and segmentation method consists of four main phases: (i) image preprocessing, (ii) image segmentation, (iii) ellipse fitting, and (iv) localisation and segmentation, as shown in Fig. 1. These phases are further divided into several steps as follows:

i. Image preprocessing: (1) colour space transformation. In this step, the input retinal image is transformed from RGB colour space to HSL colour space. Then the lightness component L is extracted to highlight the location of OD. (2) Morphological operation and median filtering. These two operations are used to remove the blood vessels of the input retinal image.
ii. Image segmentation: the vessel-free image obtained in preprocessing stage is then segmented by using the FODPSO. Since high brightness is one of the distinct features of OD, thus the retinal image can be effectively segmented according to the pixel intensity.
iii. Ellipse fitting: (1) segmented OD boundary is obtained by using the Canny edge detection. (2) Least-squares ellipse fitting is adopted to locate OD, since another distinct feature of OD is its elliptical shape.
iv. Localisation and segmentation: locating the OD according to the size of ellipse fitting region obtained in stage (iii). If the size is out of the range, the ellipse fitting region can be regarded as the OD candidate region and the FODPSO is performed again to locate OD. Otherwise, the fitting region is the final OD segmentation result. Each step is detailed and illustrated in the following sections.

3.2 Image preprocessing

As a preprocessing step, each fundus image is resized using nearest neighbour interpolation to ensure that the input retinal images can be batch processed more efficiently. Thus, the dimensions of resized images from {DRION, MESSIDOR, ORIGA} are all 600 × 400. Besides, the edges of blood vessels in retinal images may have interference on the OD segmentation. Therefore, the main purpose of image preprocessing is to remove these vessels. To achieve this goal, the input retinal image I is first transformed from RGB colour space to HSL colour space, and the lightness component L is then extracted. Next, the morphological closing operation and median filtering are performed on the L component to remove blood vessels. The above process can be written as:

$$I_{\mathrm{vf}} = \mathrm{median}_{\mathrm{sv}}(L \bullet B) = \mathrm{median}_{\mathrm{sv}}((L \oplus B)\ \Theta B) \tag{1}$$

where L is the lightness component of the HSL colour space, and B the disc-shaped structuring element that is used in the morphological closing operation. Since the OD has elliptical shape, thus the structuring element is used to preserve the circular nature of the OD. The morphological close operation is a dilation followed by an erosion operation, using the same structuring element for both operations. Next, median filtering is performed on the morphological operation result. In (1), $\oplus$ and Θ denote the operation of dilation and erosion, respectively; sv is the size of the

a *b* *c*

Fig. 2 *Removal of blood vessels*
(a) Input retinal image, ***(b)*** Lightness component image, ***(c)*** Vessel-free image

Step 1 Initialize α , ρ_1 , ρ_2 , ρ_3 // fractional coefficient, global, local and neighborhood weights
Step 2 Initialize N , $N_{\min}$, $N_{\max}$ // initial, minimum and maximum number of particles within each swarm
Step 3 Initialize N^s , $N^s_{\min}$, $N^s_{\max}$ // initial, minimum and maximum number of swarm
Step 4 Initialize Δv // maximum number of levels, a particle can travel between iterations
Step 5 Initialize I_T , I_{kill} // total number of iterations and maximum stagnation of swarms
Step 6 Initialize $0 \le x_0^n \le P-1$ // initial position of all particles from all swarms
Step 7 Initialize $\tilde{x}_t^n$, $\tilde{g}_t^n$ and $\tilde{n}_t^n$ based on x_t^n // initial local best, global best and neighborhood best of all swarms
Step 6 For each iteration *t* until I_T
For each particle *n* of swarm *s*
Update the particle velocity according to Eq. (3);
Update the location of particle: $x_{t+1}^n = x_t^n + v_{t+1}^n$;
Compute the between-class variance $\sigma_B^{c^2}$ of each RGB component *c* for each particle *n* of swarm *s*
If $\sigma_{n_B}^{c^2} > \sigma_{nbest_B}^{c^2}$ // particle *n* has improved
$\sigma_{nbest_B}^{c^2} = \sigma_B^{c^2}$
$\tilde{x}_t^n = \tilde{x}_{t+1}^n$
For each swarm *s*
If $\max \sigma_{s_B}^{c^2} > \varphi^c$ // swarm *s* has improved
$\varphi^c = \max \sigma_{s_B}^{c^2}$
$\tilde{g}_t^n = x_{t+1}^n$
$I_k = 0$ // reset stagnancy counter
If $N_s < N_{\max}$ // the current number of particles within swarm *s* is inferior to the maximum number of allowed particles
$N_s = N_s + 1$
Randomly spawns a new particle in swarm *s*
If $N^s < N^s_{\max}$ and $rand() N_s / N_{\max} > rand()$ // small probability of creating a new swarm
$N^s = N^s + 1$
Randomly spawns a new swarm with an initial number of *N* particles.
Else // swarm *s* has not improved
$I_k = I_k + 1$
If $I_k = I_{kill}$ // swarm *s* has improved for too long
If $N_s > N_{\min}$ // swarm *s* has currently more than the minimum number of allowed particles to form a swarm
Delete worse particle in swarm *s*, *i.e.* lower local solution
Else // swarm *s* does not currently have the minimum number of allowed particles to form a swarm
Delete whole swarm *s*, *i.e.*, all particles in swarm *s*
End

Fig. 3 *Algorithm 1: The FODPSO used for image segmentation*

square window used in the median filter, and I_{vf} represents the smoothed vessel-free result.

Fig. 2 shows the vessel-free result of an input retinal image. Note that the morphological operation and the median filtering operation are used here to enhance the object of interest and get rid of some curvilinear structure, since the above two operations achieve significant removal of the intensity irregularity introduced by the vessels in the OD region, thereby leading to a smoothing effect, as shown in Fig. 2*c*.

3.3 Image segmentation based on FODPSO

Retinal image segmentation involves portioning a retinal image into groups of pixels, which are homogeneous with respect to same predicate [5]. Since one of the distinct features of OD is its high brightness and the blood vessels around OD usually appear dark, thus the grey level variation in the OD region is generally higher than that in any other part of the fundus image. Based on the property, the OD region can be segmented by using the FODPSO [8, 9].

In 1995, Kennedy and Eberhart [25] introduced PSO algorithm. However, the classical PSO algorithm has some limitations, i.e. the algorithm may get stuck in a suboptimal solution region [26, 28]. Therefore, many works have been done to solve this problem. For example, Tillett *et al.* [26] introduced the Darwinian PSO (DPSO) where natural selection is employed to avoid local optima by extending classical PSO into multiple swarms, and each one performs just like ordinary PSO search.

In order to further improve DPSO, some researchers have proposed fractional-order DPSO or FODPSO [8, 24]. For instance, the fractional calculus based on the Grünwald–Letnikov concept of fractional differential [30] is used to control the convergence rate of DPSO. The fractional differential α of a given signal $x(t)$ can thus be defined as:

$$D^{\alpha}[x(t)] = \frac{1}{T^{\alpha}} \sum_{k=0}^{r} \frac{(-1)^k \Gamma(\alpha+1) x(t-kt)}{\Gamma(k+1)\Gamma(\alpha-k+1)} \tag{2}$$

where Γ, T, and r represent the gamma function, the sampling period, and the truncation order, respectively. Next, suppose $w = 1$, $T = 1$, and $r = 4$, thus the differential derivative of (2) can be written as [9, 29–31]:

$$\begin{aligned} v_{t+1}^n = {} & \alpha v_t^n + \frac{1}{2}\alpha v_t^n + \frac{1}{6}\alpha(1-\alpha)v_{t-2}^n + \frac{1}{24}\alpha(1-\alpha)(2-\alpha)v_{t-3}^n \\ & + \rho_1 r_1(\tilde{g}_t^n - x_t^n) + \rho_2 r_2(\tilde{x}_t^n - x_t^n) + \rho_3 r_3(\tilde{n}_t^n - x_t^n) \end{aligned} \tag{3}$$

For (3), when $\alpha = 1$, the equation represents classical DPSO. Besides, the parameter α controls the memory of the particles. For instance, when $\alpha < 1$, particles ignore their previous search, and the particles may be sometimes trapped in local solutions. In contrast, when $\alpha > 1$, particles will explore new solutions. Therefore, the performance of these particles will be improved under this condition.

For image segmentation, the key step is to find different threshold scales to maximise the object function of different between-class variance. The pseudo-code of the FODPSO method that is used for image segmentation is presented in Algorithm 1 (see Fig. 3). Each particle *n*, within each different swarm *s*, moves in a space according to position x_t^n and velocity v_t^n, where $0 \le x_t^n \le P-1$, and P is the intensity levels in each RGB components. The position and velocity values are highly dependent on the local best $\tilde{x}_t^n$, global best $\tilde{g}_t^n$, and the neighbourhood best $\tilde{n}_t^n$ information.

The above three PSO-based segmentation algorithms were tested on a large quantity of retinal images to determine the most effective algorithm for the application. An illustrative example is shown in Fig. 4. As can be seen in the figure, the contour of the segmentation result obtained by FODPSO seems more accurate than the results obtained by the other two algorithms. Besides, to quantitatively evaluate these segmentation results, the performance of each PSO-based segmentation algorithm is also assessed by computing the structural similarity index (SSIM) [32]. SSIM index

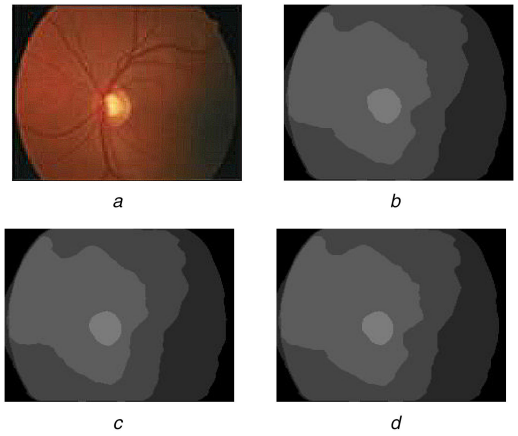

Fig. 4 *Segmentation results obtained by three PSO-based algorithms*
(a) Input image, ***(b)*** PSO result, ***(c)*** DPSO result, ***(d)*** FODPSO result

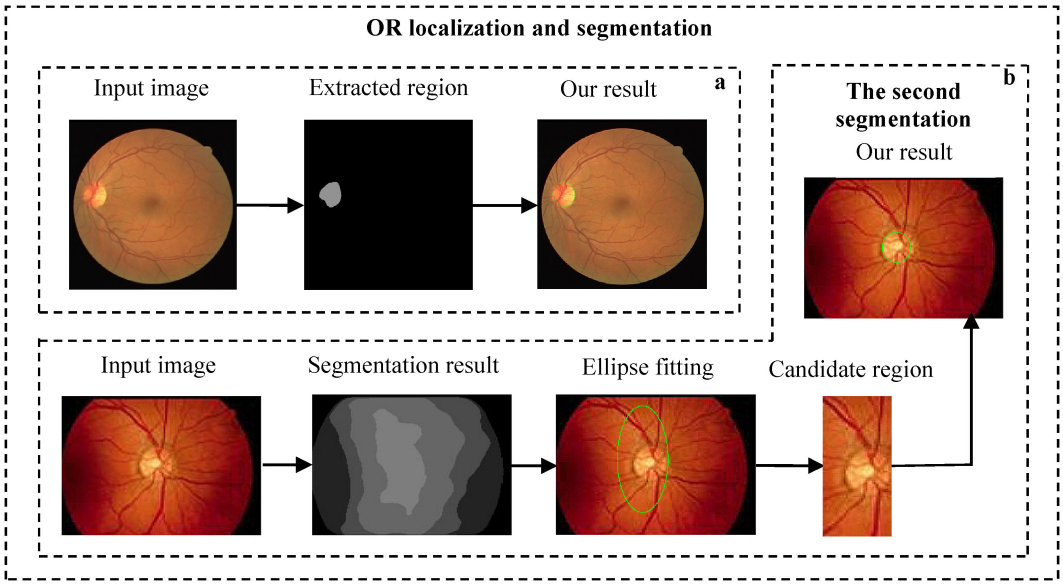

Fig. 5 *OD localisation and segmentation*
(a) Locating the OD by performing segmentation just once, ***(b)*** Locating the OD by performing segmentation twice

measures the similarity between two images. The input retinal image is regarded as an image of perfect quality, and the SSIM index can thus be viewed as a quality measure of the segmentation results obtained by the PSO-based algorithms. For the SSIM index, the higher value of the index, the better quality of the segmentation result. For the illustrative example shown in Fig. 4, the values of SSIM index obtained by PSO, DPSO, and FODPSO for segmenting an input retinal image are 0.5990, 0.5981, and 0.5992, respectively. Although these index values are close, the FODPSO algorithm yields the best result among the three PSO-based segmentation algorithms. This confirms our observation in Fig. 4. As can be seen in the figure, the FODPSO captures the lamination variation and segments region boundary more accurate than other PSO-based algorithm. The same conclusion can be also drawn by testing a large quantity of retinal images. Furthermore, the FODPSO has been proven in the literature to outperform the traditional PSO and DPSO [20]. Therefore, the FODPSO is adopted in the proposed algorithm to obtain the highest intensity region as the OD location.

3.4 Ellipse fitting and OD segmentation

Once the highest intensity region is detected by using FODPSO, we then extract the region contour so as to provide a set of contour pixels for ellipse fitting. This extraction step is performed by means of a Canny edge detector. Since another distinct feature of OD is its elliptical shape, we then use the least-squares optimisation to fit the segmented OD contour with an ellipse [2, 10]. After performing ellipse fitting, the OD can be located according to the size of ellipse fitting region. That is because generally the OD only takes up ∼5% of the whole retinal image [33]. Specifically, let M designate the height of the input image and a denote the long-axis length of the fitted ellipse. The OD can be located and segmented once for all, providing the following condition has been fulfilled:

$$2a < \frac{1}{3}M \tag{4}$$

Otherwise, the ellipse fitting region obtained by the brightness-based segmentation may be regarded as the OD candidate region, and the FODPSO is performed on the candidate region once again to locate the OD. Some illustrative examples are shown in Fig. 5. From Fig. 5, we can deduce that the OD in some retinal images can be directly located by using the FODPSO-based segmentation only once, while other retinal images need twice segmentation to correctly locate OD. The first time is to find the candidate region, and the second time is to limit the searching area just in the candidate region. Thus, the narrowed region ensures more accurate results. Finally, the centroid (y_c, x_c) and the long/short-axis length of the OD, which are obtained by ellipse fitting are used to overlay ellipse on the input image to segment OD of the input retinal image. The smooth OD borders that generate in this step can be used for cup-to-disc ratio computation, which is very important for glaucoma analysis.

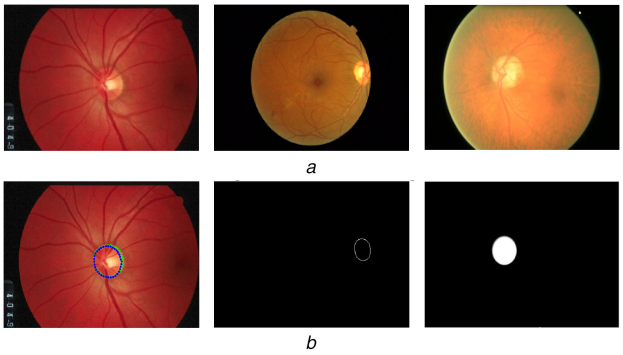

Fig. 6 *Original retinal images and associated expert annotations for OD. From left to right: DRION database, MESSIDOR database, and ORIGA database*

(a) Original retinal images, ***(b)*** Expert annotations for OD

4 Experimental results

Localisation and segmentation experiment of OD in retinal imaging are presented in this section.

First, we introduce the used public database and the assessment indexes that are used for result evaluation of OD localisation and segmentation, and then we compare our algorithm with other existing methods for the retinal images in the public databases. Finally, the quantitative evaluation is carried out to verify the effectiveness of the proposed method.

All the segmentation methods are implemented in MATLAB. The experiments are performed on a PC with 3.00 GHz Intel Pentium Dual-Core Processor.

4.1 Material

Three public databases DRION, MESSIDOR, and ORIGA are used to verify the effectiveness of the proposed algorithm. The reason why we choose the three databases is that these data sets contain not only the original retinal images, but also the associated expert annotations of OD. Therefore, they are suitable for evaluating the performance of different OD segmentation algorithms, as shown in Fig. 6.

The DRION database [34] has 110 retinal images, and the resolution of each image is 600 × 400 pixels. A colour analogical fundus camera was used to capture the retinal images. All these images were stored in JPG format and approximately centred on the optic nerve head (ONH). Independent contours from two medical experts were collected by using a software tool provided for image annotation. In each image, each expert traced the contour by selecting the most significant papillary contour points and using the annotation tool to connect automatically adjacent points by a curve. Therefore, the contour of this data set traced by the two experts can be used as the ground truth to facilitate the algorithm performance analysis.

The MESSIDOR database [35] contains 1200 colour fundus images. All these images were captured using a colour 3CCD camera on a TopconTRCNW6 nonmydriatic retinograph with a 45° FOV. The image size of the database is 2240 × 1488 pixels. The University of Huelva, Spain [1], kindly provides the OD boundary reference standard for the 1200 images. Thus, the OD boundary reference standard can be used for performance evaluation for different algorithms.

The ORIGA database [36] has 650 images from the Singapore Malay Eye Study. These images are given in JPG format with a size of 3072 × 2048 pixels per image, and the manual OD markings are given in the MATLAB MAT file.

4.2 Parameter adjustment

Several parameters are involved in the proposed method, viz., (i) size of structural element in morphological operation, (ii) size of median filter kernel, and (iii) number of segmentation level in FODPSO.

For the size of structural element in morphological operation, in our experiment, we find that image erosion with a small structuring element can disintegrate the OD into several small bright regions with low compactness, while a large structuring element can enlarge the OD boundary, thereby leading to incorrect OD boundary segmentation.

Additionally, the window size of median filter also affects the exact object boundary. Here, we analyse 50 images from the preprocessing data set to identify an optimal radius of structuring element and window size of median filtering for retinal images. It is noteworthy that the bright region obtained by thresholding the lightness component of an input retinal image with an ideal radius of the disc-shaped structuring element and a proper window size of median filter will maximise the number of bright pixels detected as OD, and minimise the number of non-OD pixels. In our experiments, we observe that for a retinal image with a size of 600 × 400, when the radius of the disc-shaped structuring element is set to be 4 pixels and the window size of median filter is set to be 20 × 20, the OD boundary can be well preserved with little unwanted effect in most cases. The reason why we choose the disc-shaped structural element and the above parameter values is that the shape of the blood vessel is round tube, and the width of the vessel in retinal images is generally no more than 20 pixels. Thus, the blood vessel may be effectively removed by these preprocessing operations.

For the number of segmentation level in FODPSO, it is found that when the level value of segmentation is too small (e.g. 2, 3) for an image with a size of 600 × 400, the OD region may be mixed with around non-OD regions due to lack of enough intensity discrimination. However, if the level value is too large (e.g. 9, 10), the OD region may be further divided without integrity, and the running time also increases gradually. Experimental results show that when the level value is set to be 5, the OD segmentation is proved to be effective and efficient in most cases.

Besides, in our experiment, each input retinal image is resized to 600 × 400 to ensure that they can be batch processed more efficiently, since the image sizes in the three public databases are all approximately equal to 3:2. However, for other fundus images with totally different sizes, fixing the input image size to 600 × 400 may affect in the aspect ratio of OD and thus influencing OD localisation and segmentation stage. Therefore, the image size should be proportionately changed in this case to ensure a correct aspect ratio of OD.

4.3 Comparative study

Some representative OD localisation and segmentation algorithms, such as blood vessel-based method [14], active contour-based method [18], and ScPSO-based method [21], are compared in this subsection with our proposed method. The reasons for choosing the three OD segmentation methods are that the first method is one of the representative model-based methods, the second method is one of the representative appearance-based methods, and the third method identifies OD using the variant of PSO algorithm just like the proposed algorithm. However, in our experiment, we find that there is no method can solve all problems, and each kind of method has its own drawbacks.

For the blood vessel-based method [14], the convergence of the blood vessels is used to locate the OD. For the method, the vessel network is first segmented and the resultant binary image is pruned to keep the main arcade. Then, the centroid of the arcade is located and the brightest area is detected to determine the position of the OD with respect to the centroid. Next, the algorithm adjusts the centroid point iteratively until it reaches the centre of the arcade and the centre is presumed to be the vessel convergence point and the centre of the OD. However, the algorithm is controlled by some parameters, and different segmentation results are obtained with different parameter values. Fig. 7 shows an example of OD segmentation results obtained by the blood vessel-based method [14] and the proposed method. One can clearly see that similar segmentation results can be obtained by using the two methods. Observation on other test images also confirms this conclusion. However, the blood vessel-based method requires retinal vessel

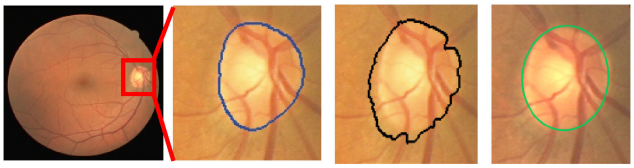

Fig. 7 *Comparison between the OD segmentation results of the blood vessel-based method and the proposed method*
(a) Input retinal image, ***(b)*** Ground truth image, ***(c)*** Segmentation result obtained by using the blood vessel-based method, ***(d)*** Segmentation result obtained by using the proposed method

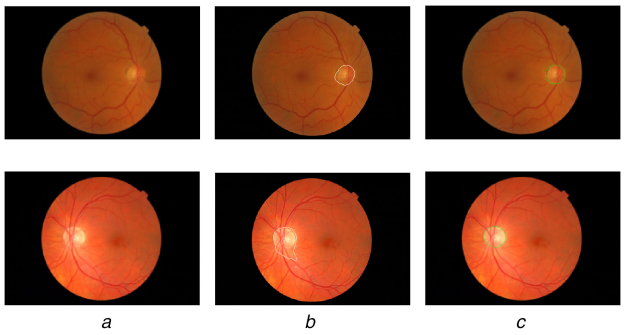

Fig. 8 *Comparison between the OD segmentation results of the active contour-based method and the proposed method*
(a) Input images, ***(b)*** Segmentation results obtained using active contour-based method, ***(c)*** Segmentation results obtained by the proposed method

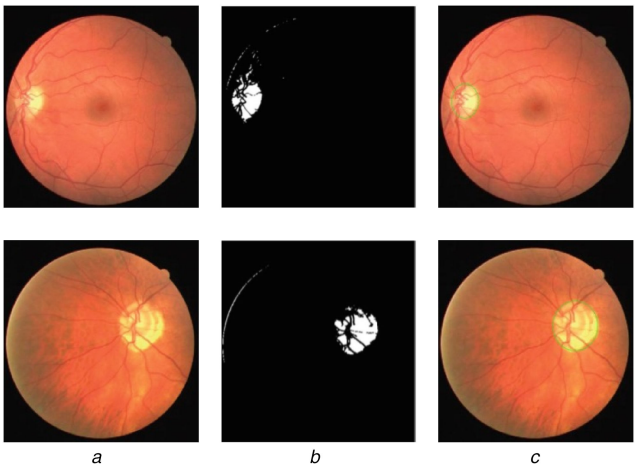

Fig. 9 *Comparison between the OD segmentation results of the ScPSO-based method and the proposed method*
(a) Input images, ***(b)*** Segmentation results obtained by the ScPSO-based method, ***(c)*** Segmentation results obtained by the proposed method.

segmentation as the initial step. Thus, the method needs relatively long time to process a retinal image. Besides, the method involves some parameters that need to be manually tuned according to different input images. In contrast, our proposed method does not need any blood vessel information in advance. The proposed method takes ∼6 s on average to process a retinal image with a size of 600 × 400, and the OD can be automatically segmented without any user-interaction for different input retinal images.

For the active contour-based method [18], the main advantage is its processing speed. The method only takes ∼22 s to process a retinal image with a size of 600 × 400, which is faster than the blood vessel-based method. However, the active contour-based method may fail in the presence of uneven brightness images. Fig. 8 shows such an example. The input image in the second row is suffered by the non-uniform luminance round OD region. In this situation, the active contour-based method is unable to provide a reliable brightest area for generating the region of interest. That is because the method is based on the pixel intensity to detect OD candidate region and the threshold value for the candidate region extraction is hard to determine when the input image has uneven brightness. On the contrast, thanks to the FODPSO that is used for grouping the input image into regions with same intensity and the ellipse fitting that is adopted to detect elliptical OD shape, our proposed method can more accurately locate the OD. Figs. 8*b* and *c* show the OD segmentation results obtained by the active contour-based method and our method, respectively. One can clearly see that our algorithm can deal with the challenge of non-uniform luminance, and better quality results can be obtained by using the proposed method for the input retinal images shown in Fig. 8*a*. However, in the experiments, we also find that although the parametric active contour method may fail due to abrupt intensity observation, shape constraint or more stringent hyper-parameter may help in getting better results.

For the ScPSO-based method [21], a cascade multithresholding process is proposed by using the ScPSO algorithm. Kapur function is used as the cost function in the method. Performance analysis shows that the ScPSO-based method obtains a high accuracy rate on OD segmentation. However, the method has also some limitations: (i) user-interaction is needed to adjust the algorithm parameters according to different input images; and (ii) the method needs a supporter technique, which achieves to only OD area without any noise or without other part of retina [21]. Fig. 9 shows the comparison results for the ScPSO-based method and our method. The ScPSO-based method obtains the OD with little noise, since the original images own some dark regions inside. Thus, these dark regions affect the optimal threshold values. Besides, blood vessels also cause a negative effect on the obtainment of threshold. By two-step multithresholding of the method, these handicaps can be minimised, as shown in Fig. 9*b*. Inspired by the work, the proposed algorithm also applies a two-step strategy to locate the OD region more accurately. This two-step strategy of our method is depicted in Figs. 5*a* and *b*. Thus, a robust segmentation process of OD in retinal images can be ensured by the proposed method with no user-interaction, as shown in Fig. 9*c*.

4.4 Quantitative evaluation

To quantitatively assess different OD segmentation methods, the centroid difference (D) for DRION database, the overlapping ratio (R) for MESSIDOR database, and the overlap score (S) for ORIGA database are used to measure the accuracy of various OD localisation and segmentation methods.

For DRION database, the difference between the x- or y-coordinate of the ground truth centroid and that of the estimated centroid obtained by OD segmentation algorithms [37] is used for comparison. Here, the centroid of the OD boundary obtained by two experts from the DRION database is used as the ground truth centroid. Let C_{gx} and C_{ex} be the x-coordinate of the ground truth centroid and the estimated centroid, and C_{gy} and C_{ey} be the y-coordinate of the above two centroids, thus the centroid difference D_x and $D_y$for the two experts ($i = 1, 2$) can be written as:

$$D_x^i = \left| C_{gx}^i - C_{ex}^i \right| \tag{5}$$

$$D_y^i = \left| C_{gy}^i - C_{ey}^i \right| \tag{6}$$

Fig. 10 shows the comparison between the x-coordinates C_{gx} and C_{ex} and the y-coordinates C_{gy} and C_{ey} of the centroids provided by the two experts and the proposed method, respectively. From the figure, one can see that the ground truth and the detected OD centres have a high positive correlation, which means the results obtained by our method are very similar to that of the expert annotations.

For MESSIDOR database, we compute the overlapping ratio [38] between the segmented OD areas A_{s} obtained by OD segmentation algorithms and the reference standard OD regions A_{g} provided by the MESSIDOR database. The overlapping ratio R can be defined as:

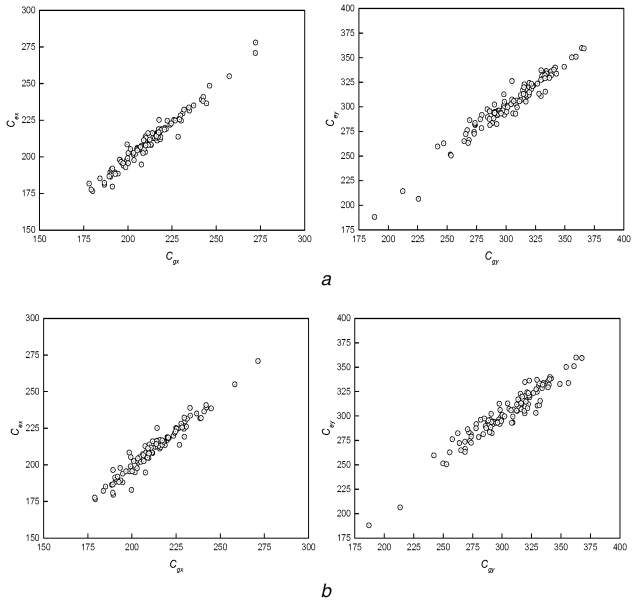

Fig. 10 *Scatter plot diagram depicts the comparison of the ground truth and the estimated centroids for the two experts*

(a) Comparison of ground truth centroid and the estimated centroid for expert1's data, ***(b)*** Comparison of ground truth centroid and the estimated centroid for expert2's data

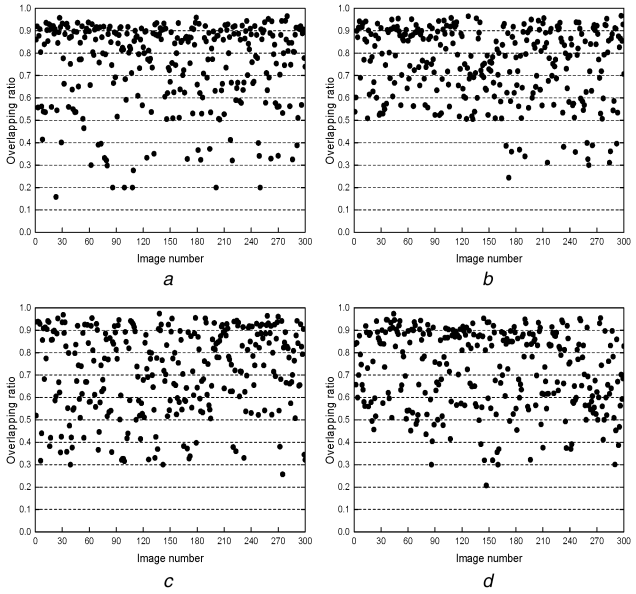

Fig. 11 *Overlapping ratio for the 1200 images in MESSIDOR database using the proposed method*

(a) Group #1, ***(b)*** Group #2, ***(c)*** Group #3, ***(d)*** Group #4

Table 1 Performance comparison for different segmentation methods

Method	R, %	D_x	D_y
blood vessel-based [14]	72.85	0.3415	0.3460
active contour-based [18]	63.71	0.5172	0.5897
ScPSO-based [21]	59.74	—	—
proposed algorithm	89.69	0.3108	0.3246

$$R = \frac{A_s \cap A_g}{A_s \cup A_g} \tag{7}$$

Fig. 11 shows the distribution of the overlapping ratio on MESSIDOR database using the proposed method. The database contains 1200 retinal images, these images are divided into 4 groups and each group has 300 images, as shown in Fig. 11.

According to the suggestions in [38], the result with at least 50% overlapping ratio can be regarded as a successful segmentation. Since it can be obtained from the figure that for 89.7% of the images in MESSIDOR database using our method achieved successful segmentation, thus we can deduce that the proposed algorithm can achieve promising OD segmentation results and is useful for clinical work.

Besides, to quantitatively assess different OD segmentation algorithms, the above centroid difference and the overlapping ratio are adopted here. For these algorithms, the result with a high overlapping ratio R and a low centroid difference value D represents a good segmentation. Table 1 shows the comparison with the above representative OD segmentation methods in terms of R and D. Note that the ScPSO-based method just segments OD from retinal images without ellipse fitting process. Therefore, the centroid difference index value is not calculated for this method. From Table 1, one can clearly see that our method achieved the highest overlapping ratio and the minimum centroid difference value. It means that better quality results may be obtained by using our method compared to the other methods.

For ORIGA database, the overlap score (S) [39] is used as the distribution of performance metric here. According to (7), the overlapping ratio (R) denotes the fraction of overlapping area between the manually annotated OD and segmented OD. Based on the R index, the S index is defined as a significant indicator of OD segmentation accuracy. The higher S value in each overlapping interval denotes better automated segmentation. Analysis of the S metric distribution on the ORIGA database is shown in Table 2. One can see that the proposed method has the highest percentage of the images with $S \geq 0.5$, and the lower percentage of the images with $S \geq 0.8$ compared to the other three methods. Examples of the best and worst OD segmentation performance obtained using the proposed algorithm on the images from ORIGA database are shown in Fig. 12.

We also compare the performance of the proposed method with that of existing algorithms shown in Table 3 for different image databases, i.e. STARE, DIARETDB1, DRIVE, and DRION. The overlapping ratio (R), success percentage (Succ), and running time (T) of the proposed algorithm are compared with the results of the existing methods. In Table 3, the performance measure of existing OD segmentation methods are directly gotten from the websites or their published papers.

The success (Succ) is one of the most important criteria in measuring the performance of OD segmentation algorithms. The success index represents the percentage of images in a particular database where OD is successfully identified ($R \geq 0.5$). The comparative analysis showing in Table 3 shows that the proposed algorithm can achieve a relatively good performance. As can be seen in Table 3, our method gives better overlapping ratio (R) than most other algorithms for various databases. The methods outperform our method in terms of Succ only by Youssif *et al.* [12] (0.9880), Foracchia *et al.* [7] (0.9750), and Salazar-Gonzalez *et al.* [14] (0.9750). However, these methods depend mainly on extracting the blood vessels of the input retinal images, they thus have the common limitation of most model-based methods, i.e. the vessel extraction phase takes relatively long time. Also, the running

Table 2 Performance of images in particular overlapping intervals on ORIGA database

Method	$S \geq 0.9$	$S \geq 0.8$	$S \geq 0.7$	$S \geq 0.5$
blood vessel [14]	31.71	54.92	86.74	90.17
active contour [18]	20.38	44.61	76.92	76.15
ScPSO-based [21]	17.64	36.93	65.82	84.63
proposed algorithm	28.52	41.08	80.54	91.31

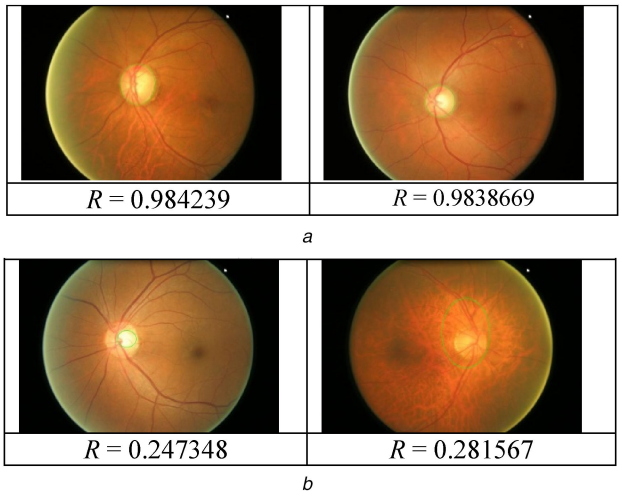

Fig. 12 *Best and worst OD segmentation performances achieved using the proposed algorithm*
(a) Best results, ***(b)*** Worst examples

Table 3 Performance measurement for different OD segmentation methods

No	Type	Methods	Database	R	Succ	T
1.	model-based method	Youssif [12]	STARE	—	0.9880	3.5 min
2.		Foracchia [7]	STARE	—	0.9750	2 min
3.		Lalonde [13]	STARE	0.8000	0.7160	1.6 s
4.		Salazar-Gonzalez [14]	DIARETDB1	0.7574	0.9670	1.2 min
			DRIVE	0.7070	0.9750	1.8 min
5.		Hoover [15]	STARE	—	0.8900	15 s
6.	appearance-based method	Tjandrasa [17]	DRIVE	0.7556	0.8673	—
7.		Nugroho [18]	DRION	0.6531	0.9271	22.7 s
8.		Mahfouz [3]	STARE	—	0.9260	0.46 s
9.		Koyubcu [21]	DRIVE	0.5789	0.9559	7-8 s
10.		proposed	DRION MESSIDOR ORIGA	0.8927	0.9287	6.9 s
				0.8169	0.8970	6.7 s
				0.7978	0.9131	6.4 s

time of the three methods is all >1 min per image. The proposed method is different from the model-based methods, since the blood vessel is not required for locating the OD region in our method. Therefore, it can give good segmentation performance at relatively fast speed. Besides, apart from the fast computational speed, the strength of the proposed method also lies in its high automaticity and reliability, since our method can automatically segment OD for different input images and the shape and location of the OD can be also effectively detected based on the two distinct features of OD.

4.5 Algorithm complexity

The computational efficiency is also an important issue for OD localisation and segmentation. Therefore, in this subsection, we will discuss the algorithm complexity of the proposed method.

In the proposed method, the most time-consuming operation is using the FODPSO algorithm to obtain the OD candidate region, and other operations, such as image preprocessing and ellipse fitting, have relatively little influence on the final algorithm complexity. Thus, here we mainly analyse the complexity of the FODPSO from two aspects: memory complexity and computational complexity. Suppose r denotes the given number of previous iterations, the FODPSO requires memorising the previous r iterations to compute a new velocity at time $t+1$. Furthermore, the computational requirements increase linearly with r. Thus, the FODPSO presents an $O(r)$ memory complexity [40]. The computational complexity of the FODPSO requires an initial computation that depends on the size of the image. After that initial set-up, the computational complexity of the FODPSO will increase with the number of desired thresholds m, and it also depends on the accumulated number of particles within each swarm, *i.e.* $\sum_{\forall s} N^s$ [41], where N^s is the initial number of swarm s. Therefore, the computational complexity of the FODPSO can be written as $O(m\sum_{\forall s} N^s)$.

CPU processing time is also an important measurement for evaluating algorithm complexity. In our experiments, we find that the FODPSO sometimes requires less CPU processing time for image segmentation in comparison to PSO and DPSO, while sometimes, it still need more time than the DPSO. That is because a high level of exploitation of FODPSO may allow a good short-term performance but will also sometimes slow down the convergence in order to reach a more feasible solution. For the proposed FODPSO-based OD segmentation algorithm, the average running time is generally ~6.72 s for an image with a size of 640 × 576 in Matlab environment. Table 3 presents the running time of different OD segmentation methods. The average running time of the proposed method for the input retinal images with different image sizes is shown in Table 4, from which one can see that the average running time rises from 4.21 to 9.46 s as the input image size increases. This speed may be further improved by more efficient image segmentation methods or a GPU-based parallel algorithm.

5 Discussion

In this section, we mainly discuss some critical issues, such as technique challenges, limitations, and possible solutions that relate to the technique contribution of the proposed method. Localisation and segmentation of OD face many technique challenges. Although some approaches have been taken to solve the problem using blood vessel-based method or active contour-based method, they still have some limitations. For example, the blood vessel-based

Table 4 Average running time of the proposed method for different size of images

Image size	Time, s	Image size	Time, s
100 × 90	4.21	300 × 270	5.44
450 × 405	5.90	600 × 400	6.41
800 × 720	7.91	1000 × 900	9.46

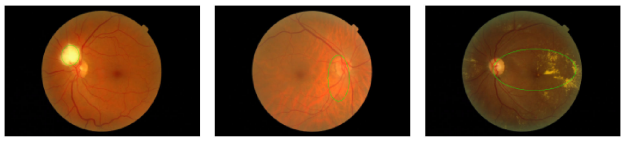

a *b* *c*

Fig. 13 *Some failure examples*

method requires retinal vessel segmentation as the initial step of the OD localisation process, thus the method is usually very time-consuming. In contrast, the running speed of the active contour-based method is faster. However, the OD outline depicted by the method seems not very promising. Therefore, a new OD localisation and segmentation method is proposed in this paper to cope with these problems, and the experimental results show that the proposed method can detect the OD with relatively high accuracy and fast speed.

However, the proposed algorithm also has the same limitations appeared in the appearance-based methods, and it may lead to invalid result in some situations: (i) the presence of retinal pathologies that alter the appearance of the OD significantly or have similar properties to the OD, as shown in Fig. 13*a*; (ii) a retinal image may be unevenly illuminated or poorly focused, resulting in a less distinct and blurred OD, as shown in Fig. 13*b*; (iii) the presence of bright lesions such as hard exudates, which have similar pixel intensity and colour characteristics with the OD, as shown in Fig. 13*c*. Nevertheless, we provide a new way to solve the OD segmentation problem based on the distinct features of OD, and the result appears to be quite successful in most cases.

In the future, we intend to investigate the following possible solutions to enhance the flexibility of the proposed OD localisation and segmentation algorithm: (i) incorporating the cup-to-disc ratio measures into the proposed scheme; (ii) choosing more proper method based on the distinct features of OD to improve the efficiency and accuracy of the OD segmentation; (iii) further minimising the computation times to meet the needs of practical requirements; (iv) developing an interactive OD localisation and segmentation software tool for ophthalmologists; (v) testing our algorithm on larger image databases and cooperating with clinical partners.

6 Conclusion

In this paper, we proposed an effective algorithm for locating and segmenting OD in retinal images. Key features of the proposed method are based on the observations that the OD in a healthy retinal image usually appears as a bright yellowish and elliptical object. Thus, the FODPSO is used to extract the brightest region and the ellipse fitting is adopted to detect elliptical OD shape in the proposed method. There are several advantages in the proposed method compared with the other existing algorithms. First, the proposed method does not need segmenting blood vessel in advance; thus, it is more efficient than the blood vessel-based method. Second, the proposed method can automatically segment OD without any user-interaction for different input retinal images. Finally, two distinct features of OD are adopted in the proposed method to more accurately detect the shape and location of the OD. Therefore, the proposed method could be suitable for automatic retinal disease screening in a variety of clinical settings.

7 Acknowledgments

This work was supported in part by the National Natural Science Foundation of China (nos. 71271215, 71221061, 61502537, 61573380, 61702558, 61602527), the Collaborative Innovation Center of Resource-conserving and Environment-friendly Society and Ecological Civilization, the International Science & Technology Cooperation Program of China (2011DFA10440), Postdoctoral Science Foundation of Central South University (No. 126648), Hunan Provincial Natural Science Foundation of China (2018JJ3681, 2017JJ3416), and China Postdoctoral Science Foundation (2017M612585).

References

[1] Devasia, T., Jacob, P., Thomas, T.: 'Automatic optic disc localization and segmentation using swarm intelligence', *World Comput. Sci. Inf. Technol. J.*, 2015, **5**, (6), pp. 92–97

[2] Yu, H., Barriga, E.S., Agurto, C., *et al.*: 'Fast localization and segmentation of optic disk in retinal images using directional matched filtering and level sets', *IEEE Trans. Inf. Technol. Biomed.*, 2012, **16**, (4), pp. 644–657

[3] Mahfouz, A.E., Fahmy, A.S.: 'Fast localization of the optic disc using projection of image features', *IEEE Trans. Image Process.*, 2010, **19**, (12), pp. 3285–3289

[4] Youssif, A., Ghalwash, A., Ghoneim, A.: 'Optic disc detection from normalized digital fundus images by means of a vessels direction matched filter', *IEEE Trans. Med. Imaging*, 2008, **27**, (1), pp. 11–18

[5] Niemeijer, M., Ginneken, B., terHaar, F.: 'Automatic detection of the optic disc, fovea and vascular arch in digital color photographs of the retina'. Proc. of the British Machine Vision Conf., Oxford, UK, 2005, pp. 109–118

[6] Li, H., Chutatape, O.: 'Automatic feature extraction in color retinal images by a model based approach', *IEEE Trans. Biomed. Eng.*, 2004, **51**, (2), pp. 246–254

[7] Foracchia, M., Grisan, E., Ruggeri, A.: 'Detection of optic disk in retinal images by means of a geometrical model of vessel structure', *IEEE Trans. Med. Imaging*, 2004, **23**, (10), pp. 1189–1195

[8] Blancher, L., Krooshof, P.W.T., Posrma, G.J., *et al.*: 'Discrimination between metastasis and glioblastoma multiforme based on morphometric analysis of MR images', *Am. J. Neuroradiol.*, 2011, **32**, (1), pp. 67–73

[9] Lahmiri, S.: 'Glioma detection based on multi-fractal features of segmented brain MRI by particle swarm optimization techniques', *Biomed. Signal Proc. Control*, 2017, **31**, pp. 148–155

[10] Liao, M., Zhao, Y.Q., Li, X.H., *et al.*: 'Automatic segmentation for cell images based on bottleneck detection and ellipse fitting', *Neurocomputing*, 2016, **173**, (3), pp. 615–622

[11] Winder, R.J., Morrow, P.J., Mcritchie, I.N., *et al.*: 'Algorithms for digital image processing in diabetic retinopathy', *Comput. Med. Imaging Graph.*, 2009, **33**, (8), pp. 608–622

[12] Youssif, A., Ghalwash, A.Z., Ghoneim, A.: 'Optic disc detection from normalized digital fundus images by means of a vessels' direction matched filter', *IEEE Trans. Med. Imaging*, 2008, **27**, (1), pp. 11–18

[13] Lalonde, M., Beaulieu, M., Gagnon, L.: 'Fast and robust optic disk detection using pyramidal decomposition and Hausdorff-based template matching', *IEEE Trans. Med. Imaging*, 2001, **20**, (11), pp. 1193–1200

[14] Salazar-Gonzalez, A.G., Lim, Y.M., Liu, X.H.: 'Optic disc segmentation by incorporating blood vessel compensation'. Proc. of IEEE Third Int. Workshop on Computational Intelligence in Medical Imaging, Paris, France, 2011, pp. 1–8

[15] Hoover, A., Goldbaum, M.: 'Locating the optic nerve in a retinal image using the fuzzy convergence of the blood vessels', *IEEE Trans. Med. Imaging*, 2003, **22**, (8), pp. 951–958

[16] Li, H., Chutatape, O.: 'Automated feature extraction in color retinal images by a model based approach', *IEEE Trans. Biomed. Eng.*, 2004, **51**, (2), pp. 246–254

[17] Tjandrasa, H., Wijayanti, A., Suciati, N.: 'Optic nerve head segmentation using Hough transform and active contour', *Telkomnika*, 2012, **10**, (3), pp. 531–536

[18] Nugroho, H.A., Listyalina, L., Setiawan, N.A., *et al.*: 'Automated segmentation of optic disc area using mathematical morphology and active contour'. Proc. of Int. Conf. on Computer, Control, Informatics and Its Applications, Bandung, Indonesia, 2015, pp. 18–22

[19] Sopharak, A., Uyyanonvara, B., Barman, S.: 'Automatic exudate detection from non-dilated diabetic retinopathy retinal images using fuzzy C-means clustering', *Sensors*, 2009, **9**, pp. 2148–2161

[20] Ghamisi, P., Couceiro, M.S., Benediktsson, J.A., *et al.*: 'An efficient method for segmentation of images based on fractional calculus and natural selection', *Expert Syst. Appl.*, 2012, **39**, (16), pp. 12407–12417

[21] Koyuncu, H., Ceylan, R.: 'Optic disk segmentation with Kapur-ScPSO based cascade multithresholding'. Proc. of Int. Conf. on Bioinformatics and Biomedical Engineering, Granada, Spain, 2016, pp. 206–215

[22] Krishna, M., Jayashree, R., Lakshmi, M.V.: 'Segmentation of retina-based on fractional PSO technique', *Int. J. Advanced Res. Comput. Commun. Eng.*, 2013, **2**, (3), pp. 1384–1387

[23] Dorigo, M., Maniezzo, V., Colorni, A.: 'Ant system: optimization by a colony of cooperating agents', *IEEE Trans. Syst., Man, Cybernetics, Part B (Cybernetics)*, 1996, **26**, (1), pp. 29–41
[24] Kennedy, J., Eberhat, R.: 'Particle swam optimization'. Proc. of the IEEE Int. Conf. on Neural Network, Perth, Western Australia, 1995, pp. 1942–1948
[25] Kennedy, J., Eberhat, R.: 'A new optimizer using particle swarm theory'. Proc. of the IEEE Sixth Int. Symp. on Micro Machine and Human Science, Indianapolis, USA, 1995, pp. 39–43
[26] Tillett, J., Rao, T.M., Sahin, F.*, et al.*: 'Darwinian particle swarm optimization'. Proc. of the 2nd Indian Conf. on Artificial Intelligence., Pune, India, 2005, pp. 1474–1487
[27] Couceiro, M.S., Martins, F.M.L., Rocha, R.P.*, et al.*: 'Mechanism and convergence analysis of a multi-robot swarm approach based on natural selection', *J. Intell. Robot. Syst.*, 2014, **76**, (2), pp. 353–381
[28] Couceiro, M.S., Rocha, R.P., Ferreira, N.M.F.*, et al.*: 'Introducing the fractional-order Darwinian PSO', *Signal, Image Video Process.*, 2012, **6**, (3), pp. 343–350
[29] Xie, W.Y., Li, Y.S.: 'An automatic fractional coefficient setting method of FODPSO for hyperspectral image segmentation', *Proc. SPIE*, 2015, **9501**, pp. 1–9
[30] Ghamisi, P., Couceiro, M.S., Benediktsson, J.A.: 'Extending the fractional order Darwinian particle swarm optimization to segmentation of hyperspectral images', Proc. SPIE, 2012, **8537**, pp. 1–11
[31] Wang, D.S., Wang, H.T., Liu, L.: 'Unknown environment exploration of multi-robot system with the FORDPSO', *Swarm Evol. Comput.*, 2016, **16**, pp. 157–174
[32] Wang, Z., Bovik, A.C., Sheikh, H.R.*, et al.*: 'Image quality assessment: from error visibility to structural similarity', *IEEE Trans. Image Process.*, 2004, **13**, (4), pp. 600–612
[33] Jonas, J.B., Budde, W.M.., Panda, J.S.: 'Ophthalmoscopic evaluation of the optic nerve head', *Surv. Ophthalmol.*, 1999, **43**, (4), pp. 293–320
[34] Carmona, E.J., Rincon, M., Carcia-Feijoo, J.*, et al.*: 'Identification of the optic nerve head with genetic algorithms', *Artif. Intell. Med.*, 2008, **43**, (3), pp. 243–259
[35] Decenciere, E., Zhang, X., Cazuguel, G.*, et al.*: 'Feedback on a publicly distributed image database: the Messidor database', *Image Anal. Stereol.*, 2014, **33**, (3), pp. 231–234
[36] Cheng, J., Zhang, Z., Tao, D.*, et al.*: 'Similarity regularized sparse group lasso for cup to disc ratio computation', *Biomed. Optics Express*, 2017, **8**, (8), pp. 3763–3777
[37] Aquino, A., Gegundez-Arias, M.E., Marin, D.: 'Detecting the optic disc boundary in digital fundus images using morphological, edge detection, and feature extraction techniques', *IEEE Trans. Med. Imaging*, 2010, **29**, (11), pp. 1860–1869
[38] Niemeijer, M., Abramoff, M.D., Ginneken, B.v.: 'Segmentation of the optic disc, macula and vascular arch in fundus photographs', *IEEE Trans. Med. Imaging*, 2007, **26**, (1), pp. 116–127
[39] Roychowdhury, S., Koozekanani, D.D., Kuchinka, S.N.*, et al.*: 'Optic disc boundary and vessel origin segmentation of fundus images', *IEEE J. Biomed. Health Inform.*, 2016, **20**, (6), pp. 1562–1574
[40] Couceiro, M., Ghamisi, P.: '*Fractional order Darwinian particle swarm optimization – applications and evaluation of an evolutionary algorithm*' (Springer International Publishing, AG Switzerland, 2016)
[41] Ghamisi, P., Couceiro, M.S., Martins, F.M.L.*, et al.*: 'Multilevel image segmentation based on fractional-order Darwinian particle swarm optimization', *IEEE Trans. Geosci. Remote Sensing*, 2014, **52**, (5), pp. 2382–2394